Three Mask Polysilicon Thin Film Transistor Biosensor

K.Sun, I.Zeimpekis, M.Lombardini, N.M.J.Ditshego, S.J.Pearce, K.S.Kiang, O.Thomas, M.R.R.de Planque, H.M.H.Chong, H.Morgan, P.Ashburn

***Abstract*— Biosensors are commonly produced using an SOI CMOS process and advanced lithography to define nanowires. In this work, a simpler and cheaper junctionless 3-mask process is investigated, which uses thin film technology to avoid the use of SOI wafers, in-situ doping to avoid the need for ion implantation and direct contact to a low doped polysilicon film to eliminate the requirement for heavily doped source/drain contacts. Furthermore, TiN is used to contact the biosensor source/drain because it is a hard, resilient material that allows the biosensor chip to be directly connected to a printed circuit board without wire bonding. pH sensing experiments, combined with device modelling, are used to investigate the effects of contact and series resistance on the biosensor performance, as this is a key issue when contacting directly to low doped silicon. It is shown that in-situ phosphorus doping concentrations in the range 4×10^{17} cm^{-3} to 3×10^{19} cm^{-3} can be achieved using 0.1% PH_3 flows between 4 and 20 sccm. Furthermore, TiN makes an ohmic contact to the polysilicon even at the bottom end of this doping range. Operation as a biosensor is demonstrated by the detection of C-Reactive Protein (CRP), an inflammatory biomarker for respiratory disease.**

***Index Terms*—Biosensor, pH sensor, Plasma CVD, Semiconductor device fabrication, Thin film transistors**

I. Introduction

Over the past decade, silicon nanowires have been widely researched for application as biochemical sensors [1]-[12]. Silicon nanowires are of interest for a number of reasons, for example a high surface-to-volume ratio gives high sensitivity and electrical sensing gives real-time, label-free detection without the use of expensive optical components. Initial research used bottom-up self-assembly [1], [2] for nanowire fabrication, which involves the use of a metal catalyst to grow the nanowires. A nanowire alignment technology is also needed, such as electric field or fluid-flow-assisted nanowire positioning to locate the nanowires between lithographically defined source and drain electrodes [3]. The bottom-up approach has the advantage of simplicity, but precise control of nanowire size and position is very difficult. Top-down approaches overcome these shortcomings, and several groups have used advanced lithography techniques to fabricate single-crystal silicon nanowires on silicon-on-insulator (SOI) wafers [4]-[9]. This has the advantage of CMOS compatibility for the development of sensor systems, but a serious disadvantage is the high cost associated with advanced lithography techniques and expensive SOI wafers.

Low-cost manufacture is critically important for nanowire biosensor applications because for widespread uptake of biosensors in Point of Care settings, the biosensor needs to be disposable and hence very cheap. Several groups [10]-[12] have researched top-down approaches that do not need advanced lithography by using coarser lithography and specialist wet etches to reduce the nanowire diameter. However, these approaches still use expensive SOI wafers and have the disadvantage that wet etches are generally not favored for manufacturing. An alternative to CMOS-based nanowire technologies is to use Thin Film Transistor (TFT) technology on non-SOI substrates, as is widely used for the manufacture of displays. This approach offers the prospect of very low cost, because displays are mass manufactured as large panels (2.88 meter × 3.13 meter for Sharp 10^{th} generation), which are then cut to smaller sizes for application in TV, computer and mobile phone screens. This gives a very low cost per unit substrate area. Several groups [13]-[16] have reported top-down approaches for the fabrication of polysilicon nanowires using variants of thin film transistor technology. In our previous work [15] we reported a technology for producing rectangular polysilicon nanowire biosensors and demonstrated the detection of two inflammatory biomarkers, the proteins interleukin-8 and tumor necrosis factor-alpha, over a wide range of concentrations and with excellent sensitivity.

In this paper, we report a very simple junctionless polysilicon Thin Film Transistor biosensor (TFT biosensor) for application in Point of Care diagnostics that can be fabricated with just three masks for polysilicon definition, metallization and sensing window definition. This small mask count has been achieved by using a thin in-situ low doped polysilicon layer without any highly doped contact regions. pH sensing is used to assess biosensor performance and device modelling is performed to assess the effect of contact resistance. The

Manuscript received for review November 28, 2013.The authors would like to acknowledge the Technology Strategy Board (TSB) and the Engineering and Physical Sciences Research Council (EPSRC: EP/K502327/1) for funding this work. We would also like to thank Ben Hadwen, Sally Anderson, Greg Gay and Jason Hector of Sharp Laboratories Europe for many useful discussions.

K.Sun, I.Zeimpekis, M. Lombardini, N.M.J.Ditshego, S.J. Pearce, K. S. Kiang, M. R. R. de Planque, H. M. H. Chong, H. Morgan, and P. Ashburn are with the Electronics & Computer Science, University of Southampton, Southampton, SO17 1BJ, UK (e-mail: ks5@ecs.soton.ac.uk).

O.Thomas is with Oxford Instruments Plasma Technology, Yatton, Bristol, BS49 4AP, UK (e-mail: Owain.THOMAS@oxinst.com).

K.Sun and I. Zeimpekis contributed equally to this work.

Operation of the TFTs as biosensors is demonstrated by the sensing of the inflammatory biomarker C-Reactive Protein (CRP) in buffer solution. The TFT biosensor technology is compatible with thin film transistor display technology and hence highly manufacturable.

II. Experimental Procedure

The Thin Film Transistor (TFT) biosensor fabrication technology is illustrated schematically in Fig. 1. N-type <100> silicon wafers were used as substrate. A 100 nm silicon dioxide layer was then grown by wet thermal oxidation and a 300 nm silicon nitride layer deposited by low pressure chemical vapour deposition. A 45 nm amorphous silicon layer was then deposited at 200ºC using an Oxford Instruments Plasma Technology PlasmaPro 100 Plasma Enhanced Chemical Vapor Deposition (PECVD) system. In-situ doping was achieved using 0.1% PH_3 gas and the flow rate was varied between 4 and 40 sccm, while the SiH_4, and H_2 flows were both kept constant at 100 sccm and Ar flow was varied between 296 and 260 sccm to fix a total gas flow of 500 sccm. The process pressure was set at 800 mTorr and the RF power at 10 W. The first lithography step (Fig. 1(a)) was used to define the TFT biosensor geometry and an 8.5 nm gate oxide was then grown at 900ºC in O_2 to create a gate insulator for the liquid gate. This gate oxidation also crystallized the amorphous silicon into polycrystalline silicon and activated the phosphorus dopant.

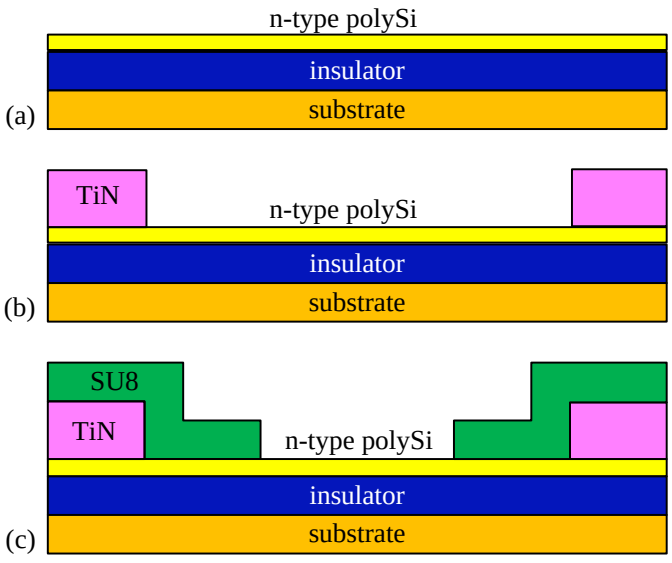

Fig. 1. Schematic illustration of the three mask Thin Film Transistor (TFT) biosensor fabrication for (a) poly-Si formation and patterning, (b) TiN sputtering and lift-off and (c) SU-8 passivation and sensing window formation.

The second lithography step was used to define the metallization patterns prior to metal deposition and lift-off. TiN was chosen for the metallization because it is a hard, resilient material [17] that can easily be connected to a printed circuit board using a SAMTEC SEI series connector (Fig. 2(a)) without the need for packaging and wire bonding. The TiN was deposited by sputtering after removal of the gate oxide from the contact areas using 20:1 buffered HF (Fig. 1(b)). The third photolithography step is needed to open a sensing window in an SU8 layer so that liquid can be applied to the TFT biosensor (Fig. 1(c)) without overlapping onto the TiN contacts. The devices produced through this fabrication process do not include heavily doped source/drain areas or pn junctions and are therefore junctionless TFTs. To investigate the effect of source/drain pads, some devices were produced with heavily doped n+ source/drain regions. These n+ contacts were produced using a separate in-situ doped polysilicon layer deposited at 200ºC using 10% PH_3, SiH_4, H_2 and Ar gases at a flow rate of 2 sccm, 50 sccm, 100 sccm and 348 sccm. Fig. 2(b) shows an optical micrograph of the completed TFT biosensor.

The pH measurements were made using a liquid gate, with a Ag/AgCl electrode biased at 10 mV and a source/drain bias of 100 mV, as shown in Fig. 2(c). The low liquid gate bias was chosen to avoid electrolysis in the buffer solution and to minimize any leakage current, while keeping the device in the subthreshold region. The substrate was kept at ground for all electrical measurements. To demonstrate the operation of the low doped TFT as a biosensor, low doped TFT biosensors were functionalized with anti-CRP antibody to create a biosensor for CRP sensing. The surface of the TFT was then exposed to increasing concentrations of CRP molecules suspended in 0.1mM phosphate buffer (pH7).

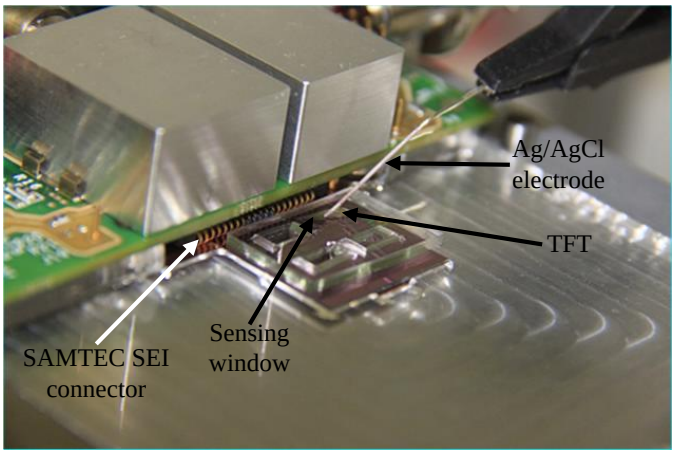

(a)

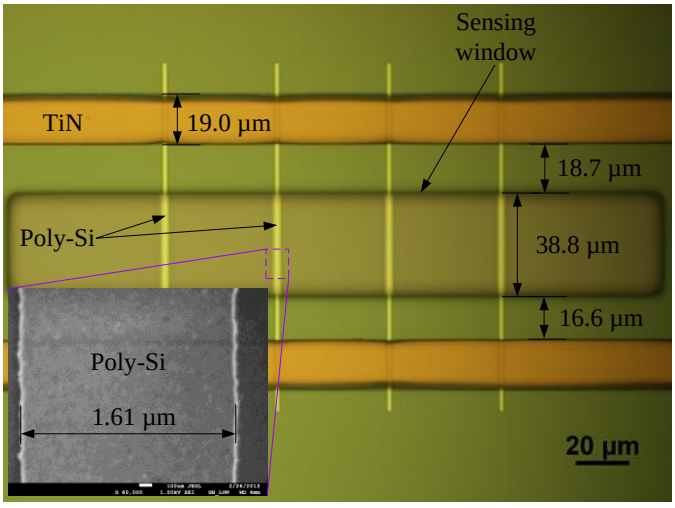

(b)

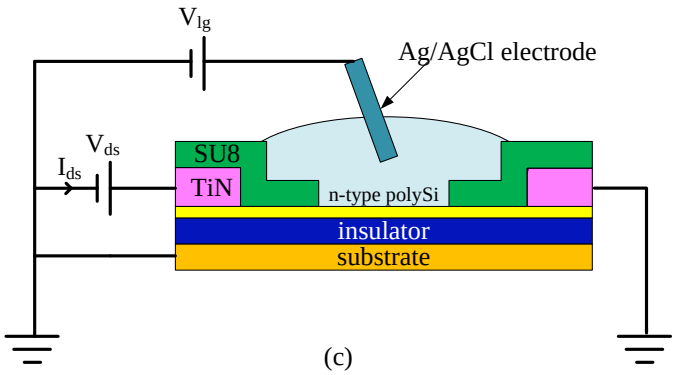

Fig. 2. Photographs and schematic of (a) biosensor system, (b) chip and (c) test configuration. The inset in Fig. 2(b) shows a scanning electron microscope image of the polysilicon layer.

The electrical results obtained in air on the TFT biosensor were interpreted using Silvaco Atlas device simulations [18]. To simulate the polysilicon layer, a uniform doping profile and a 1.1 µm grain size was assumed, with 10 nm grain boundaries (in a real layer, there can be large variations in grain size and orientation). The grains were assumed to be defect-free and all defects were incorporated in the grain boundaries using the default defect model parameters. The simulations used the Lombardi (CVT) mobility model and the Shockley-Read-Hall (SRH) recombination model.

III. Results & Discussion

The sheet resistance of the amorphous silicon was measured by four-point-probe and was found to be very high after deposition at 200ºC, indicating that dopant activation is very low. However, after gate oxidation at 900ºC the sheet resistance decreases dramatically. Fig. 3 shows the sheet resistance after a 900°C oxidation as a function of PH_3 flow. A sheet resistance of 140 kΩ/sq is obtained for a PH_3 flow of 4 sccm, which then drops to 1.8 kΩ/sq for a PH_3 flow of 40 sccm. The Hall Effect mobility was measured on a polysilicon layer deposited using a PH_3 flow of 20 sccm and a value of 29 cm^2/Vs was obtained. Using this value of mobility, an average doping concentration of around 4×10^{17} cm^{-3} is estimated for a PH_3 flow of 4 sccm and around 3×10^{19} cm^{-3} for a PH_3 flow of 20 sccm.

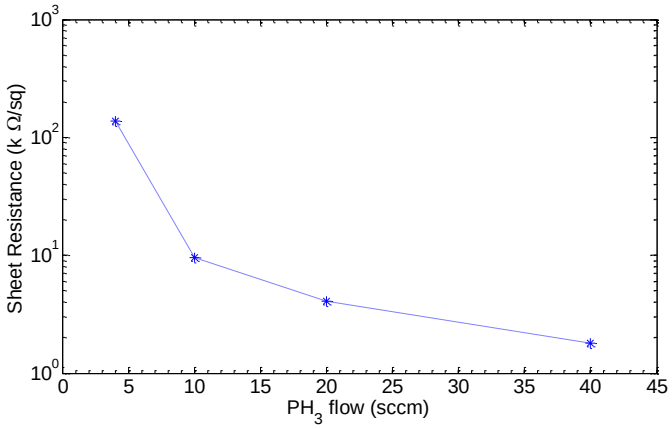

Fig. 3. Sheet resistance as a function of PH_3 flow for in-situ doped polysilicon layers deposited as amorphous silicon at 200ºC and then annealed at 900ºC for 10 minutes in dry O_2 to crystallize to polysilicon and activate the phosphorus dopant.

Fig. 4 shows current/voltage characteristics measured in air (no V_{lg}) for low doped (PH_3 flow of 4 sccm) and high doped (PH_3 flow of 20 sccm) TFT biosensors. The characteristic of the low doped device in Fig. 4(a) is linear at low values of drain voltage, with a resistance of 3.3 MΩ, and then begins to saturate at higher values of drain voltage, with a resistance of 7.0 MΩ at a drain bias of 15 V. In contrast, the characteristic of the high doped device in Fig. 4(b) is linear at all values of drain voltage, with a resistance of 59 kΩ. The linearity of the characterization at low bias in Fig. 4 strongly suggests that the TiN contacts are ohmic.

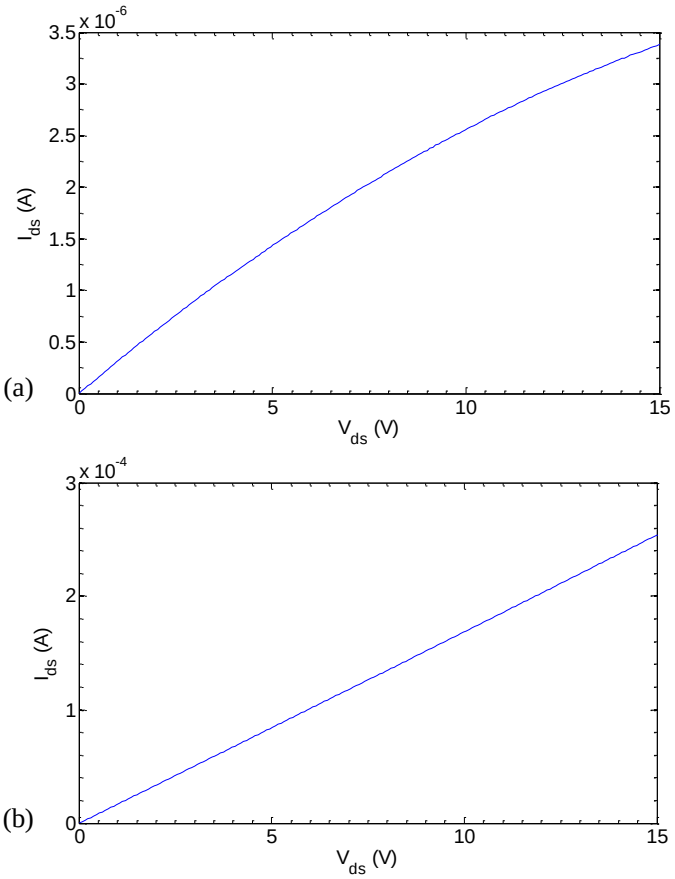

Fig. 4. Graph of drain/source current as a function of drain/source voltage for (a) a low doped junctionless TFT biosensor and (b) a high doped junctionless TFT biosensor. The low doped biosensor was produced using a PH_3 flow of 4 sccm and the high doped biosensor using a PH_3 flow of 20 sccm. The channel was 74 µm and the width was 6.4 µm. No n+ source/drain pads were used on the biosensors.

To gain an indication of the sensitivity of the TFT biosensor at different doping concentrations, the effect of pH on drain/source current was explored with low doped (PH_3 flow of 4 sccm) and high doped (PH_3 flow of 20 sccm) devices. Results are shown in Fig. 5, where the normalized conductance change is plotted as a function of pH for two high doped and two low doped TFT biosensors. The error bars represent the standard deviation of five consecutive measurements at the same pH. A conductance change of just below 6% is obtained at a pH of 3

for the low doped biosensor and around 4% for the high doped biosensor. This result is qualitatively as expected, since modelling shows that biosensor sensitivity is inversely proportional to the doping concentration [19].

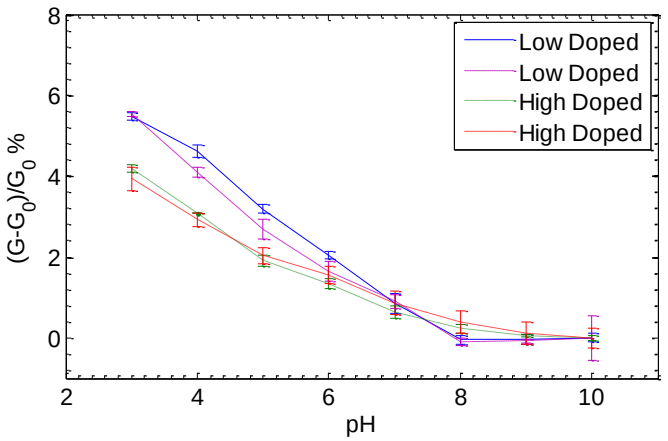

Fig. 5. Graph of normalized biosensor conductance change as a function of pH for two junctionless TFT biosensors with a low doping concentration (PH_3 flow of 4 sccm) and two with a high concentration (PH_3 flow of 20 sccm). The channel length was 74 µm and the width was 6.4 µm. No n+ source/drain pads were used on the biosensors.

When the polysilicon doping is low, it is difficult to make low resistance, ohmic contacts. To determine the effect of the contact regions, the normalized conductance change in the TFT as a function of pH for TFTs with and without heavily doped source/drain pads was explored. The observed changes are plotted in Fig. 6. At a pH of 3, a normalized conductance change of just below 9% is obtained on TFT biosensors with heavily doped source/drain pads, compared with just below 6% for junctionless biosensors without the n+ source/drain pads. This result confirms that the contact regions are degrading the performance of the biosensor.

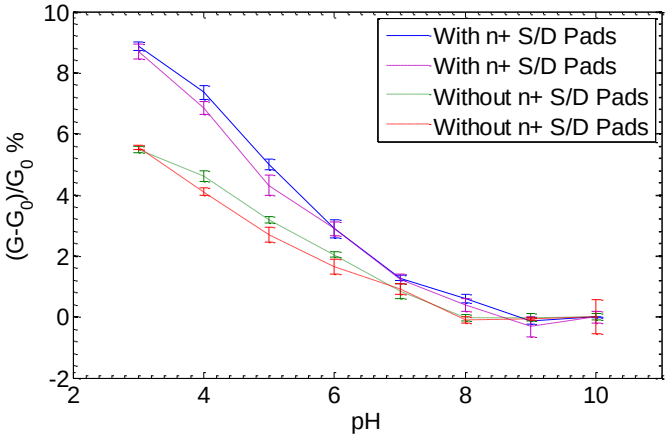

Fig. 6. Graph of normalized biosensor conductance change as a function of pH for TFT biosensors with and without n+ source/drain pads. The channel lengths were 57 µm and 74 µm for devices with and without heavily doped source/drain pads, respectively. The width for both devices is 6.4 µm.

To better understand the effect of the source/drain contact and series resistance in TFT biosensors, device simulations were performed to determine whether the TiN contacts were ohmic. This was done by defining a metal semiconductor (Schottky) contact in the device simulator and then varying the contact workfunction (φ). Measurement and simulation results are shown in Fig. 7, where it can be seen that the shape of the measured current-voltage characteristic is predicted using values of workfunction in the range 0 to 4.47 eV. When higher values of workfunction are used, strong saturation of the source/drain current is seen due to the action of the source/drain contacts that are Schottky diodes at these high values of workfunction. The simulated values of work function (up to 4.47 eV) for TiN ohmic contacts are consistent with reported values in the literature between 4.30 eV and 4.65 eV [20]. As the measured current voltage characteristics of the low doped TFT biosensor does not show strong saturation, it can be concluded that the TiN contacts in this device are ohmic. Thus the TiN contacts are ohmic even in the low doped biosensor, which has a doping concentration of around 4×10^{17} cm^{-3}.

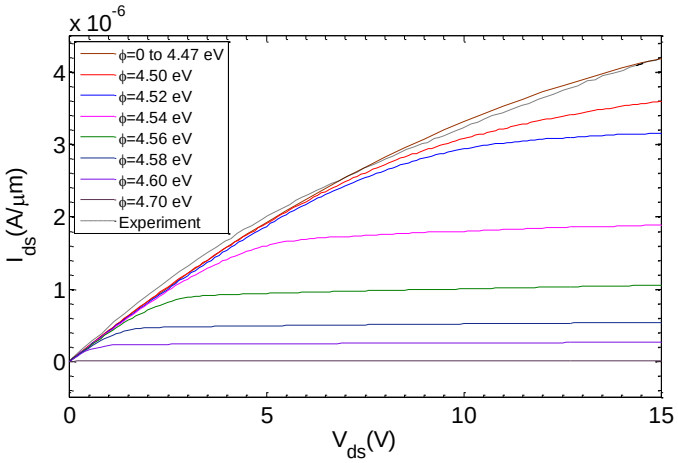

Fig. 7. Simulated current/voltage characteristics of a low doped TFT biosensor for different values of workfunction (φ) for the TiN/polysilicon contact. The simulations used a doping concentration of 1.0×10^{17} cm^{-3}, a channel length of 75 µm, a grain size of 1.1 µm, a grain boundary size of 10 nm and 71 grains between source and drain. Experimental results are shown for comparison.

Further simulations were carried out to investigate the role of grain boundaries on the TFT biosensor behavior. Fig. 8 shows simulated current/voltage characteristics of a low doped TFT biosensor for different numbers of grain boundaries. A measured current/voltage characteristic is shown along with simulation results for different numbers of grain boundaries (GB), with a simulation result for crystalline silicon as a benchmark. As expected, the biosensor current decreases as the number of grain boundaries increases because the effective mobility is reduced. This result indicates that TFT biosensors would be expected to operate at lower currents than comparable single-crystal silicon biosensors made in SOI silicon. However, if operation at a particular current level is required, this can be achieved by adjusting the width of the TFT biosensor to give the required current. It can be seen that good agreement between measured and simulated characteristics is obtained for a device with 72 grain boundaries.

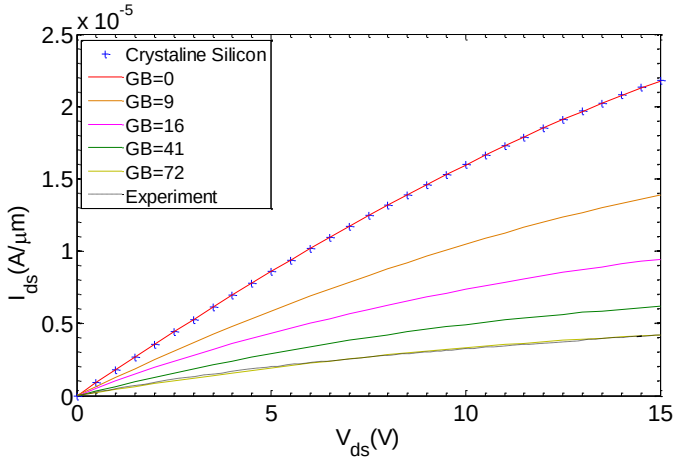

Fig. 8. Simulated current/voltage characteristics of a low doped TFT biosensor for different numbers of grains in the TFT biosensor. The simulations used a doping concentration of 1.0×10^{17} cm^{-3}, a channel length of 75 μm, a source/drain series resistance of 1.2×10^{6} Ω, a grain size of 1.1 μm, and a grain boundary size of 10 nm. Experimental results are shown for comparison and simulation results for single-crystal silicon are shown as a benchmark.

To investigate the effect of doping on the TFT biosensor behavior, current/voltage characteristics for different doping concentrations were simulated and compared with the measured current-voltage characteristics for a low doped TFT biosensor (Fig. 9). As expected, the biosensor current decreases as the doping concentration is reduced. Furthermore, the shape of the current-voltage curve becomes less linear as the doping concentration is reduced. This finding is consistent with the measured results in Fig. 4, which show a linear relationship between current and voltage for the high doped TFT biosensor but a non-linear relationship for the low doped biosensor. Good agreement between measured and simulated characteristics is obtained for a doping concentration of 1.0×10^{17} cm^{-3}. This is in reasonable agreement with the doping concentration of around 4×10^{17} cm^{-3} extracted from Fig. 3, given that the mobility model in the simulator has not been adjusted to fit the measured value of Hall mobility.

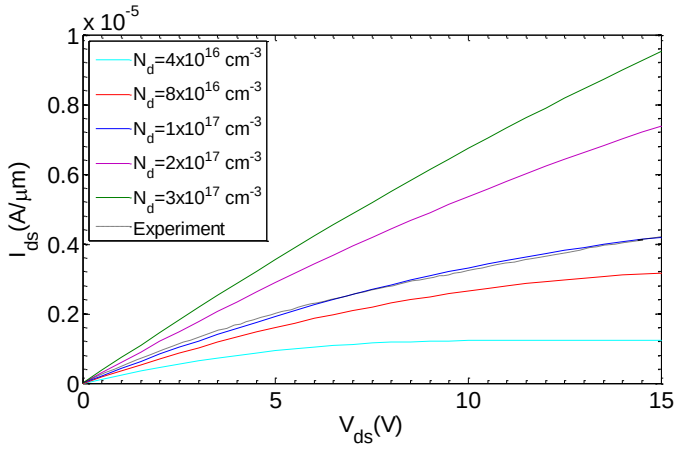

Fig. 9. Simulated current/voltage characteristics of a TFT biosensor for different channel doping concentrations (N_d). Experimental results are shown for comparison. The simulations used a channel length of 75 μm, a source/drain series resistance of 1.2×10^{6} Ω, a grain size of 1.1 μm, a grain boundary size of 10 nm and 71 grains between source and drain.

To investigate the effect of heavily doped source/drain contact and series resistance in the low doped TFT biosensor, simulations were performed in which the TiN ohmic contact was modeled as a source/drain series resistor, R_{ser}, with a fixed value. This resistor models the total resistance between the edge of the SU8 sensor window and the TiN tracks and hence includes contact resistance and the series resistance of the source/drain end regions of the TFT biosensor. Fig. 10 shows simulated current/voltage characteristics for different values of R_{ser} and for comparison measured characteristics for the low doped TFT biosensor. As expected, the biosensor current decreases as R_{ser} increases. Good agreement between measured and simulated characteristics is obtained for a value of R_{ser} around 1.2 MΩ. From the experimental results in Fig. 4(a), the total resistance of the low doped TFT biosensor varies from 3.3 MΩ at low drain bias to 7.0 MΩ at high drain bias. Since the pH measurements were taken at low drain bias, the source/drain series resistance of 1.2 MΩ can be compared with a total TFT biosensor resistance of 3.3 MΩ, which represents about 36% of the total resistance. The pH sensing results in Fig. 6 show that low doped junctionless TFT biosensors without n+ source/drain pads show a conductance change of 5.4%, compared with 8.6% with heavily doped source/drain pads, a 37% reduction. This reduction in conductance change is in excellent agreement with the simulated 36% that the contact end regions contribute to the total biosensor resistance. The reduction in conduction change during pH sensing in the low doped biosensors can therefore be explained by the series resistance of the source/drain contact regions.

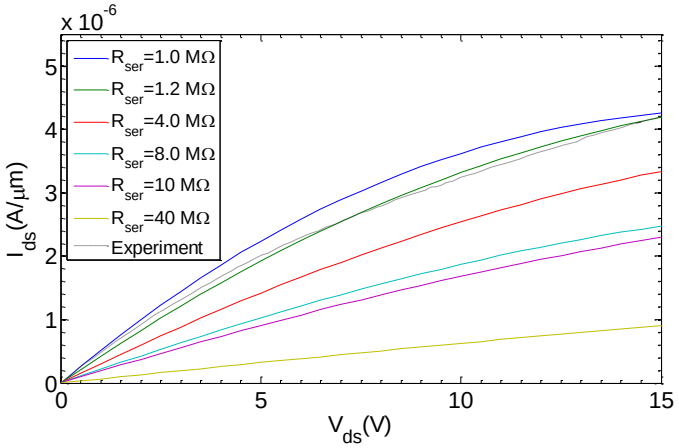

Fig. 10. Simulated current/voltage characteristics of a low doped TFT biosensor for different values of source/drain series resistance. Experimental results are shown for comparison. The simulations used a doping concentration of 1.0×10^{17} cm^{-3}, a channel length of 75 μm, a grain diameter of 1.1 μm, a grain boundary size of 10 nm and 71 grains between source and drain.

When designing a TFT biosensor, the doping concentration should be reasonably low to achieve a high sensitivity. Simulations of nanowire biosensors by Nair et al. [18] indicated that a doping concentration in the range 1×10^{17} to 1×10^{18} cm^{-3} is a suitable choice, but at this low doping concentration series resistance of the source/drain contacts will be an issue. The channel length of the biosensor should therefore be designed to give a source/drain series resistance that is a small fraction of

the total biosensor resistance. For the contact technology and doping concentration used in our low doped TFT biosensor, a channel length of 400 µm would give a device in which the series resistance of the source/drain region contributes only 5% to the total biosensor resistance. Interestingly the simulations of Nair et al. [18] predict a small increase in sensitivity with decreasing channel length. However, this benefit of channel length scaling will only be obtained if the source/drain series resistance is also scaled.

To demonstrate the operation of the low doped TFT as a biosensor, low doped TFT biosensors were functionalized with anti-CRP antibody to create a biosensor for CRP sensing. Fig. 11 (red curve) shows the percentage electric signal change (conductance change $\Delta G/G_0\%$) versus CRP concentration. The percentage conduction change is indicated in the graph as a percentage coverage change (coverage %) so that the affinity titration curve can be compared with the standard enzyme linked immunosorbent assay (ELISA) for CRP (blue curve). In this case the percentage coverage corresponds to the optical absorbance signal change of the ELISA. The standard ELISA was performed with the same concentrations of CRP suspended in the same phosphate buffer pH7 used for the electrical sensing. The agreement between the biosensor and ELISA results is reasonably good, indicating that the change in conductance seen in the TFT biosensor is consistent with protein binding.

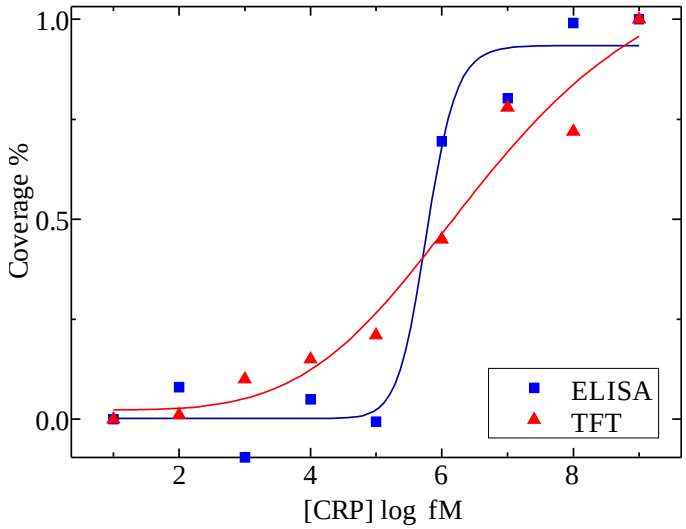

Fig. 11. Titration curve obtained using the low doped TFT biosensor for the reaction of CRP in 0.1 mM buffer (red curve). Detection of CRP using an ELISA in 0.1 mM phosphate buffer at pH7 is also shown for comparison (blue curve).

The above results have shown that a simple three mask top-down TFT process can be used to create a biosensor. This approach has the advantage over bottom-up self-assembled nanowire biosensors that the location and dimensions of the biosensor are accurately defined using photolithography. It also has the advantage over CMOS-based nanowire biosensors that there is no requirement for advanced lithography and expensive SOI wafers. However, source/drain contact and series resistance in low doped TFT biosensors degrades the sensitivity during sensing. This problem can be solved by adding heavily doped source/drain pads, but at the cost of an additional mask. As discussed above, a better approach is to design the TFT biosensor in the three mask process so that the source/drain series resistance is only a small fraction of the total resistance. This can be done by adjusting the channel length of the biosensor. It may also be possible to reduce the contact resistance by either introducing a low resistance barrier layer or by siliciding the contacts.

IV. Conclusions

In conclusion, we have presented a simple three mask technology for the fabrication of polysilicon TFT biosensors for application in Point of Care diagnostics. The polysilicon was in-situ doped to avoid the requirement for ion implantation and the three masks were polysilicon definition, metallization and sensing window definition. TiN has been used for the metallization, as it is a hard material that can be used to directly attach the biosensor chip to a printed circuit board without the requirement for wire bonding. The technology is simple and suitable for the mass manufacture of disposable biosensors.

The effect of source/drain series resistance on biosensor performance has been extensively investigated using electrical measurements, device simulations and pH sensing experiments. Electrical measurements on completed biosensors, and associated device simulations, have shown that ohmic contacts to TiN are obtained for the complete range of doping concentrations studied. To maximize the biosensor sensitivity in our three mask TFT technology, the biosensor should be designed so that the source/drain contact and series resistance is a small fraction of the total biosensor resistance. For a doping concentration around 4×10^{17} cm^{-3}, a channel length of 400 µm gives a device in which the source/drain contact and series resistance contributes only 5% to the total biosensor resistance. This channel length can be scaled provided the source/drain contact and series resistance is similarly scaled. Nevertheless, even without extensive optimization of the biosensor design, we have demonstrated that the TFT biosensor can be successfully used to sense C-Reactive Protein.

References

[1] Y. Cui, Q. Q. Wei, H. K. Park, and C. M. Lieber, "Nanowire nanosensors for highly sensitive and selective detection of biological and chemical species," Science, vol. 293, no. 5533, pp. 1289-1292, Aug. 2001.

[2] G. F. Zheng, F. Patolsky, Y. Cui, W. U. Wang, and C. M. Lieber, "Multiplexed electrical detection of cancer markers with nanowire sensor arrays," Nature Biotechnol., vol. 23, no. 10, pp. 1294-1301, Oct. 2005.

[3] W. Lu, P. Xie, and C. M. Lieber, "Nanowire Transistor Performance Limits and Applications," IEEE Trans. on Electron Devices, vol. 55, no. 11, pp. 2859-2876, Nov. 2008.

[4] Z. Li, Y. Chen, X. Li, T. I. Kamins, K. Nauka, and R. S. Williams, "Sequence-specific label-free DNA sensors based on silicon nanowires," Nano Letters, vol. 4, no. 2, pp. 245-247, Feb. 2004.

[5] Y. L. Bunimovich, Y. S. Shin, W. S. Yeo, M. Amori, G. Kwong, and J. R. Heath, "Quantitative real-time measurements of DNA hybridization with alkylated nonoxidized silicon nanowires in electrolyte solution," Journal of the American Chemical Society, vol. 128, no. 50, pp. 16323-16331, Dec. 2006.

[6] B. R. Dorvel, B. Reddy, J. Go, C. D. Guevara, E. Salm, M. A. Alam, and R. Bashir, "Silicon Nanowires with High-k Hafnium Oxide Dielectrics

for Sensitive Detection of Small Nucleic Acid Oligomers," ACS Nano, vol. 6, no. 7, pp. 6150-6164, Jul. 2012.

[7] I. Y. Park, Z. Y. Li, X. M. Li, A. P. Pisano, and R. S. Williams, "Towards the silicon nanowire-based sensor for intracellular biochemical detection," Biosens. & Bioelectron., vol. 22, no. 9-10, pp. 2065-2070, Apr. 2007.

[8] A. Tarasov, M. Wipf, K. Bedner, J. Kurz, W. Fu, V. A. Guzenko, O. Knopfmacher, R. L. Stoop, M. Calame, and C. Schonenberger, "True Reference Nanosensor Realized with Silicon Nanowires," Langmuir, vol. 28, no. 25, pp. 9899-9905, Jun. 2012.

[9] G. J. Zhang, L. Zhang, M. J. Huang, Z. H. H. Luo, G. K. I. Tay, E. J. A. Lim, T. G. Kang, and Y. Chen, "Silicon nanowire biosensor for highly sensitive and rapid detection of Dengue virus," Sensors and Actuators B-Chemical, vol. 146, no. 1, pp. 138-144, Apr. 2010.

[10] E. Stern, J. F. Klemic, D. A. Routenberg, P. N. Wyrembak, D. B. Turner-Evans, A. D. Hamilton, D. A. LaVan, T. M. Fahmy, and M. A. Reed, "Label-free immunodetection with CMOS-compatible semiconducting nanowires," Nature, vol. 445, no. 7127, pp. 519-522, Feb. 2007.

[11] M. H. Lee, K. N. Lee, S. W. Jung, W. H. Kim, K. S. Shin, and W. K. Seong, "Quantitative measurements of C-reactive protein using silicon nanowire arrays," Int J. of Nanomed., vol. 3, no. 1, pp. 117-124, Mar. 2008.

[12] S. Y. Chen, J. G. Bomer, W. G. van der Wiel, E. T. Carlen, and A. van den Berg, "Top-Down Fabrication of Sub-30 nm Monocrystalline Silicon Nanowires Using Conventional Microfabrication," ACS Nano, vol. 3, no. 11, pp. 3485-3492, Nov. 2009.

[13] H. C. Lin, M. H. Lee, C. J. Su, T. Y. Huang, C. C. Lee, and Y. S. Yang, "A simple and low-cost method to fabricate TFTs with poly-Si nanowire channel," IEEE Electron Device Lett., vol. 26, no. 9, pp. 643-645, Sep. 2005.

[14] C. Y. Hsiao, C. H. Lin, C. H. Hung, C. J. Su, Y. R. Lo, C. C. Lee, H. C. Lin, F. H. Ko, T. Y. Huang, and Y. S. Yang, "Novel Polysilicon Nanowire Field Effect Transistors for Biosensing Application," Biosens. & Bioelectron., vol. 24, no. 5, pp. 1223-1229, Jan. 2009.

[15] M. M. A. Hakim, M. Lombardini, K. Sun, F. Giustiniano, P. L. Roach, D. E. Davies, P. H. Howarth, M. R. R. de Planque, H. Morgan, and P. Ashburn, "Thin Film Polycrystalline Silicon Nanowire Biosensors," Nano Letters, vol. 12, no. 4, pp. 1868-1872, Apr. 2012.

[16] G. Wenga, E. Jacques, A. C. Salaun, R. Rogel, L. Pichon, and F. Geneste, "Step-gate polysilicon nanowires field effect transistor compatible with CMOS technology for label-free DNA biosensor," Biosensors & Bioelectron., vol. 40, no. 1, pp. 141-146, Feb. 2013.

[17] W. Wittmer, H. Melchior, "Applications of TiN thin films in silicon device technology," Thin Solid Films, vol. 93, no. 3-4, pp. 397-405, Jul. 1982.

[18] "ATLAS user's manual: Device simulation software," Silvaco, 2008.

[19] P. R. Nair, and M. A. Alam, "Design considerations of silicon nanowire biosensors," IEEE Trans. on Electron Devices, vol. 54, no. 12, pp. 3400-3408, Dec. 2007.

[20] S. A. Vitale, J. Kedzierski, P. Healey, P. W. Wyatt, and C. L. Keast, "Work-Function-Tuned TiN Metal Gate FDSOI Transistors for Subthreshold Operation," IEEE Trans. on Electron Devices, vol. 58, no. 2, pp. 419-426, Feb. 2011.